*Am J Physiol Renal Physiol* 302: F116–F128, 2012.
First published September 7, 2011; doi:10.1152/ajprenal.00184.2011.

# Hypoxia modulates the undifferentiated phenotype of human renal inner medullary CD133$^+$ progenitors through Oct4/miR-145 balance

**Benedetta Bussolati,[1] Aldo Moggio,[1] Federica Collino,[1] Giulia Aghemo,[1] Giuseppe D'Armento,[2] Cristina Grange,[1] and Giovanni Camussi[1]**

[1]*Department of Internal Medicine, Research Center for Experimental Medicine and Center for Molecular Biotechnology, and* [2]*Department of Biomedical Sciences and Human Oncology, University of Torino, Torino, Italy*

Submitted 6 April 2011; accepted in final form 6 September 2011

**Bussolati B, Moggio A, Collino F, Aghemo G, D'Armento G, Grange C, Camussi G.** Hypoxia modulates the undifferentiated phenotype of human renal inner medullary CD133$^+$ progenitors through Oct4/miR-145 balance. *Am J Physiol Renal Physiol* 302: F116–F128, 2012. First published September 7, 2011; doi:10.1152/ajprenal.00184.2011.—Low-oxygen tension is an important component of the stem cell microenvironment. In rodents, renal resident stem cells have been described in the papilla, a relatively hypoxic region of the kidney. In the present study, we found that CD133$^+$ cells, previously described as renal progenitors in the human cortex, were enriched in the renal inner medulla and localized within the Henle's loop and thin limb segments. Once isolated, the CD133$^+$ cell population expressed renal embryonic and stem-related transcription factors and was able to differentiate into mature renal epithelial cells. When injected subcutaneously in immunodeficient mice within Matrigel, CD133$^+$ cells generated canalized structures positive for renal specific markers of different nephron segments. Oct4A levels and differentiation potential of papillary CD133$^+$ cells were higher than those of CD133$^+$ cells from cortical tubuli. Hypoxia was able to promote the undifferentiated phenotype of CD133$^+$ progenitors from papilla. Hypoxia stimulated clonogenicity, proliferation, vascular endothelial growth factor synthesis, and expression of CD133 that were in turn reduced by epithelial differentiation with parallel HIF-1$\alpha$ downregulation. In addition, hypoxia downregulated microRNA-145 and promoted the synthesis of Oct4A. Epithelial differentiation increased microRNA-145 and reduced Oct4 level, suggesting a balance between Oct4 and microRNA-145. MicroRNA-145 overexpression in CD133$^+$ cells induced downrelation of Oct4A at the protein level, inhibited cell proliferation, and stimulated terminal differentiation. This study underlines the role of the hypoxic microenvironment in controlling the proliferation and maintaining a progenitor phenotype and stem/progenitor properties of CD133$^+$ cells of the nephron. This mechanism may be at the basis of the maintenance of a CD133$^+$ population in the papillary region and may be involved in renal regeneration after injury.

stem cells; microenvironment; renal regeneration; niche; renal repair

RESIDENT STEM CELLS are thought to contribute, after birth, to the growth and homeostasis of different organs and to repair tissue injury. Several studies address the presence of resident stem cells/progenitors within the adult kidney (16). In rodents, the papilla has been suggested to represent the niche for label retaining stem cells (33). In particular, in the adult mice, papillary stem cells were shown to reside in the upper papilla, where they formed "chains" of proliferating cells and to migrate into the cortex thus contributing to the homeostasis of the kidney as rapidly proliferating cells (34). The presence of stem cells capable to reenter in mitosis in response to renal injury has been described also in the renal tubules of adult rats (26, 27). In the human adult, kidney CD133$^+$ renal progenitor cells have been characterized by our group in the renal cortex from the tubule/interstitium (2). In addition, CD133$^+$/CD24$^+$ stem cells have been isolated from the Bowman's capsule (39). A genomic characterization of multipotent CD133$^+$/CD24$^+$ renal progenitor cells from glomeruli and tubules of adult human kidney revealed no significant differences in the gene expression patterns, suggesting that tubular and glomerular renal progenitor cells represent a genetically homogeneous population (40). Indeed, the presence of cytokeratin expression by the CD133$^+$/CD24$^+$ cells (39) suggests an epithelial commitment that characterizes these cells as epithelial progenitors. It is at present unknown whether in humans renal epithelial progenitors are present also in the medulla and in papilla, as described in rodents.

Recently, Humphreys et al. (17), using genetic fate mapping techniques, showed that in mice the majority of the newly generated tubular epithelial cells derived from surviving differentiated epithelial cells after ischemia-reperfusion injury, implying a role for resident cells in regeneration. It is therefore possible that regeneration mechanisms may activate proliferation of an intratubular epithelial progenitor population (12, 23), including CD133+ progenitors. Alternatively, repair may induce dedifferentiation of surviving resident cells that may acquire progenitor phenotype and contribute to regeneration. Moreover, during the regeneration of the adult kidney, several embryonic genes involved in nephrogenesis, such as Six-2 and Pax-2, are reactivated (37). However, the mechanisms involved are currently unknown. We hypothesised that properties of CD133$^+$ cells present in the nephron, such as proliferation and differentiation, might be modulated by the microenvironment, and in particular by hypoxia, possibly through transcriptional and epigenetic mechanisms known to regulate the phenotype of progenitor cells (44).

We therefore aimed to evaluate the presence of CD133$^+$ cells in different segments of the nephron, and in particular in the papilla, and their phenotype. As the renal medulla has the lowest physiologic oxygen tension compared with any other organ (15), we evaluated whether the hypoxic environment could influence the properties and phenotype of CD133$^+$ epithelial renal progenitors and the molecular mechanisms involved.

## METHODS

*Antibodies.* The following monoclonal antibodies (mAb) were used, all fluorescein isothiocyanate- or phycoerythrin-conjugated anti-CD133/1 (clone AC133) and anti-CD133/2 (clone 293C3; Miltenyi Biotech GmbH, Bergisch Gladbach, Germany); anti-CD24, -CD29,

Address for reprint requests and other correspondence: B. Bussolati, Dept. of Internal Medicine, Center for Molecular Biotechnology, Univ. of Torino, Cso Dogliotti 14, 10126 Torino, Italy (e-mail: benedetta.bussolati@unito.it).

-CD44, -CD45, -CD73, -CD90, (Becton Dickinson, San Jose, CA), anti-CD105, anti-fibroblast growth factor receptor (FGFR)4 (BioLegend, San Diego, CA), anti-met (e-Bioscience, San Diego, CA), anti-FGFR1 (Abcam, Cambridge, UK), and anti-SSEA-4 (R&D Systems, Minneapolis, MN). Fluorescein isothiocyanate- or phycoerythrin-conjugated mouse nonimmune isotypic IgGs (Miltenyi Biotech) were used as negative controls.

In addition, the following unconjugated Abs were used: anti-Pax-2 Ab (Covance, Princeton, NJ), anti-pan-cytokeratin mAb (CK, Immunological Sciences, Rome, Italy), anti-NaCl cotransporter, anti-aminopeptidase A, anti-alkaline phosphatase, anti-chloride channel CLCK-1 goat Abs (all from Santa Cruz Biotechnology, Santa Cruz, CA), and anti-Tamm-Horsfall protein (THP), anti-human HLA-I, anti-nestin, anti-megalin, anti-aquaporin (AQ)1, anti-AQ2, and anti-AQ3 rabbit Abs (all from Santa Cruz Biotechnology) and anti-vimentin mAb (Sigma). Recognition of primary antibodies was done using Alexa Fluor 488- or Texas Red-conjugated anti-rabbit, anti-mouse, or anti-goat antibodies (Molecular Probes, Leiden, Netherlands).

For Western blot analysis, the following antibodies were used: anti-Oct4 rabbit Ab (used to detect both Oct4A and Oct4B isoforms), anti-Oct4A mAb (sc-5279, recognizing the aa 1–134 of the Oct4A), anti-actin Ab (all from Santa Cruz Biotechnology), and anti-HIF-1α and anti-HIF-2α (Novus Biologicals, Littleton, CO). In experiments aimed to detect both Oct4 isoforms, Oct4A band detected with the anti-Oct4 rabbit Ab was confirmed using the anti-Oct4A mAb.

*Isolation and culture conditions.* Renal progenitor cells were obtained from the normal portion of the papillary region of the inner medulla obtained from surgically removed kidneys, after approval of the ethical committee for the use of human tissue of the university. Briefly, tissue samples of ~3–5 mm$^3$ were obtained at the papillary region of a renal pyramid. Tissue was rinsed with Hank's balanced salt solution (Sigma, St. Louis, MO) and, after being cut, digested in 0.1% collagenase type I (Sigma) for 45 min at 37°C. Tissue was subsequently forced through a graded series of meshes to separate the cell components from stroma and aggregates. The filtrate was pelleted by centrifugation. CD133$^+$ cells were isolated by magnetic cell sorting, using the MACS system (Miltenyi Biotec, Auburn, CA), as described (2), and cells were resuspended in expansion medium (EBM: medium plus supplement kit; Cambrex BioScience) without serum addition at a density of $1.0 \times 10^4$ viable cells/cm$^2$. Colonies were observed after 2–3 days and confluence was achieved 7 days after plating. Aliquots of the cell suspension were subjected to FACS analysis for quantification of CD133$^+$ cells. In selected experiments, CD133$^-$ cells or the unsorted cell population were plated in the same conditions. CD133$^+$ cells from tubuli were isolated from the cortex of the same kidney, depleted of glomeruli, as previously described (2).

To assess their capacity to generate colonies, cells were seeded using a limiting dilution technique in 96-well plates. After 12 h, wells not containing single cells were discarded by microscopical visualization and clones derived from a single cell were expanded in expansion medium. When cultured in hypoxic conditions, cells were placed in hypoxic chambers with 1% $O_2$. To evaluate the effect of hypoxia, we seeded and cultured cells in hypoxia until the clones were passaged from a 96- to a 24-well plate.

*In vitro differentiation.* Epithelial differentiation was done by culturing cells for 10 days in expansion medium with 10 ng/ml human hepatocyte growth factor (HGF; Sigma) and 20 ng/ml human FGF-4 (Sigma) (2).

*Immunofluorescence and immunohistochemistry.* For flow cytometry, cultured cells were detached with a nonenzymatic cell dissociation solution (Sigma) and blocked with RPMI containing 10% of heat-inactivated FCS. Cells were then incubated in PBS containing 0.1% BSA (Sigma) for 30 min with fluorescein isothiocyanate- or phycoerythrin-conjugated Abs. In each experimental point, 10,000 cells were analyzed on a FACScan (Becton Dickinson, Franklin Lakes, NJ).

Indirect immunofluorescence was performed on cells cultured on chamber slides. Cells, cultured until confluence on chamberslides coated with fibronectin (Sigma), were fixed in 4% paraformaldehyde containing 2% sucrose for 15 min at 4°C and, when needed, permeabilized with 0.1% Triton X-100 (Sigma) for 8 min at 4°C and then incubated overnight at 4°C with the appropriate antibodies. Indirect immunofluorescence on 10-μm cryostatic sections of human kidney was performed following the protocol described by Jászai et al. (18). Briefly, sections were incubated with 0.005% SDS in 0.2% gelatin-PBS for 30 min. The samples were then rinsed with 0.15% saponin/0.2% gelatin in PBS (S/G solution) for 30 min each and labeled overnight at 4°C with the selected antibodies. Primary antibodies were detected using appropriate secondary antibodies. Hoescht 33258 dye (Sigma) was added for nuclear staining and imaging was performed using a Zeiss SM 5 Pascal model Confocal Microscope (Carl Zeiss International). Cell expression of renal markers was analyzed semi-quantitatively by measuring fluorescence intensity by digital image analysis after subtraction of the background fluorescence of tissue, using the LSM image analysis program (Carl Zeiss International) as previously described (3). Sections from paraffin-embedded blocks of human CD133$^+$ cells placed in Matrigel in severe combined immunodeficiency (SCID) mice were collected onto poly-L-lysine-coated slides. Endogenous peroxidase activity was blocked with 6% $H_2O_2$ for 8 min at room temperature. Primary antibodies were applied to slides overnight or for 1 h at 4°C. Horseradish peroxidase-labeled anti-rabbit or anti-mouse Envision polymers (Dako) were incubated for 1 h. The reaction product was developed using 3,3-diaminobenzidine. Omis-

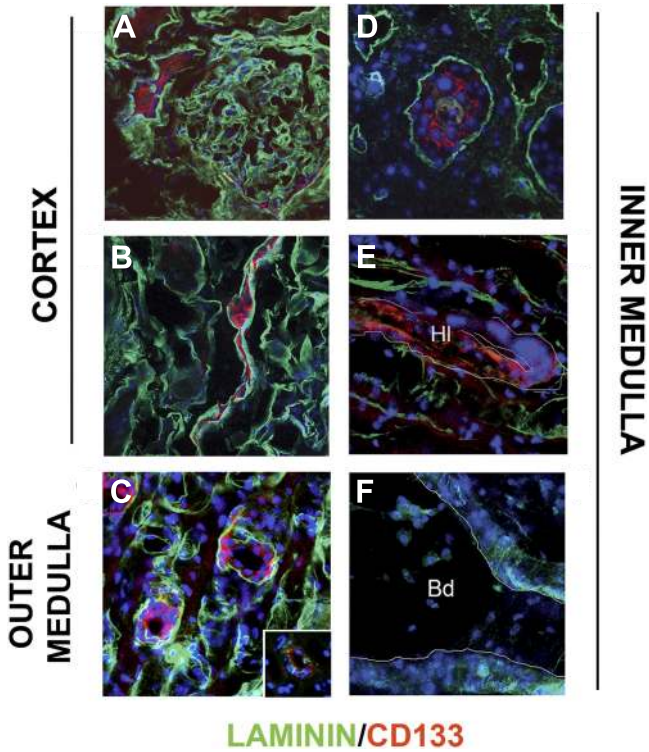


Fig. 1. Localization of CD133$^+$ cells in different regions of the normal human kidney. Representative confocal immunofluorescence micrographs showing staining of different regions of the normal human kidney with CD133 (clone AC133–1; red) and laminin (green). Cortical tissue: positive staining in the glomerular Bowman's capsule (*A*) and in some tubular cells (*A* and *B*). Outer medulla: staining of some small tubules (*C*); *inset*: costaining of CD133 (red) and CD24 (green). Inner medulla: positive staining for CD133 in some tubules (*D*) and Henle's loop (Hl; *E*) but not in the Bellini ducts (Bd; *F*). Nuclear staining was performed with Hoechst dye 33342. Original magnification ×400.

sion of the primary antibody or substitution with an unrelated rabbit serum or mouse IgG served as negative control.

*Cell proliferation assays.* CD133+ cells were seeded at 2,500 cells/well into 96-well plates in expansion medium, left to adhere overnight and starved for 12 h in RPMI (Sigma) with 2% FCS. Then, DNA synthesis was detected as incorporation of 5-bromo-2-deoxyuridine (BrdU) into the cellular DNA after 48 h of culture in expansion medium. Cells were fixed with 0.5 M ethanol/HCl and incubated with nuclease to digest the DNA. BrdU incorporated into the DNA was detected using an anti-BrdU peroxidase-conjugated antibody and visualized with a soluble chromogenic substrate, according to the manufacturer's instructions (Roche Applied Science, Mannheim, Germany). Optical density was measured with an ELISA reader (BioRad, Hercules, CA) at 415 nm (reference 495 nm). Results are the mean of five independent experiments, made in quadruplicate.

*RNA and protein analysis.* Total RNA was isolated from different cell preparations using the mirVana RNA isolation kit (Ambion) according to the manufacturer's protocol. RNA was then quantified spectrophotometrically (Nanodrop ND-1000, Wilmington, DE). For gene expression analysis, quantitative real-time PCR (qRT-PCR) was performed as previously described (7). Briefly, first-strand cDNA was produced from 200 ng of total RNA using the High Capacity cDNA Reverse Transcription Kit (Applied Biosystems, Foster City, CA). Real-time PCR experiments were performed in 20-μl reaction mixture containing 5 ng of cDNA template, the sequence-specific oligonucleotide primers (purchased from MWG-Biotech AG, Ebersberg, Germany, www.mwg-biotech.com) and the Power SYBR Green PCR Master Mix (Applied Biosystems). β-Actin or TATA-binding protein (TBP) mRNA were used to normalize RNA inputs. Fold change expression with respect to control was calculated for all samples.

For microRNA detection, 200 ng of input RNA from all samples were reverse transcribed with the miScript Reverse Transcription Kit. cDNA was then used to detect and quantify miR145 level by qRT-PCR using the miScript SYBR Green PCR Kit (all from Qiagen, Valencia, CA) (7). All samples were run in triplicate using 3 ng of cDNA for each reaction as described by the manufacturer's protocol (Qiagen). The snoRNA, RNU48 was used as normalizer. Negative controls using 10 μl of water in place of the RNA were performed alongside each reaction. Relative quantification of the products was performed using a 48-well StepOne Real-Time System (Applied Biosystems). Sequence-specific oligonucleotide primers are reported below. For protein analysis, cells were lysed at 4°C for 30 min in RIPA buffer (20 nM Tris·HCl, 150 nM NaCl, 1% deoxycholate, 0.1% SDS, 1% Triton X-100, pH 7.8) supplemented with protease and phosphatase inhibitors cocktail and PMSF (Sigma). Aliquots of the cell lysates containing 40 μg protein, as determined by the Bradford method, were run on 8% SDS-PAGE under reducing conditions and electroblotted onto PVDF membrane filters.

*Sequence-specific oligonucleotide primers.* Human Oct4A: forward, 5′-AGC AGG AGT CGG GGT GG-3′ (nt 348–364) and reverse, 5′-CTG GGA CTC CTC CGG GTT-3′ (nt 465–448); human Oct4B: forward, 5′-GC ACT TCT ACA GAC TAT TCC TTG G-3′ (nt 673–697) and reverse, 5′-AGA GCT TTG ATG TCC TGG GAC T-3′ (nt 811–790); human Oct4B1 (GenBank no. EU518650): forward, 5′-GC ACT TCT ACA GAC TAT TCC TTG G-3′ (nt 3–26) and reverse, 5′-CTT AGA GGG GAG ATG CGG TCA-3′ (nt 284–264); human Nanog: forward, 5′-ACA ACT GGC CGA AGA ATA GCA-3′ (nt 683–703) and reverse, 5′-GGT TCC CAG TCG GGT TCA C-3′ (nt 793–775); human Six1: forward, 5′-AGG CCA AGG AAA GGG AGA AC-3′ (nt 796–815) and reverse, 5′-GCT GGA CAT GAG CGG CTT-3′ (nt 893–876); human Six2 forward, 5′-CAC AGG TCA GCA ACT GGT TCA-3′ (nt 790–810) and reverse, 5′-GAG CTG CCT AAC ACC GAC TTG-3′ (nt 928–908); human Sox2 forward, 5′-TGC GAG CGC TGC ACA T-3′ (nt 727–742) and reverse, 5′-GCA GCG TGT ACT TAT CCT TCT TCA-3′ (nt 819–796); human KLF4 forward, 5′-CCA TTA CCA AGA GCT CAT GCC-3′ (nt 1683–1703) and reverse, 5′-GGG CCA CGA TCG TCT TCC-3′ (nt 1761–1744); human c-Myc forward, 5′-CAG CGA CTC TGA GGA GGA ACA-3′ (nt 1316–1336) and reverse, 5′-TGA GGA GGT TTG CTG TGG C-3′ (nt 1444–1426); human PAX-2: forward, 5′-CCC AGC GTC TCT TCC ATC A-3′ (nt 938–956) and reverse, 5′-GGC GTT GGG TGG AAA GG-3′ (nt 1002–986); human ANG-

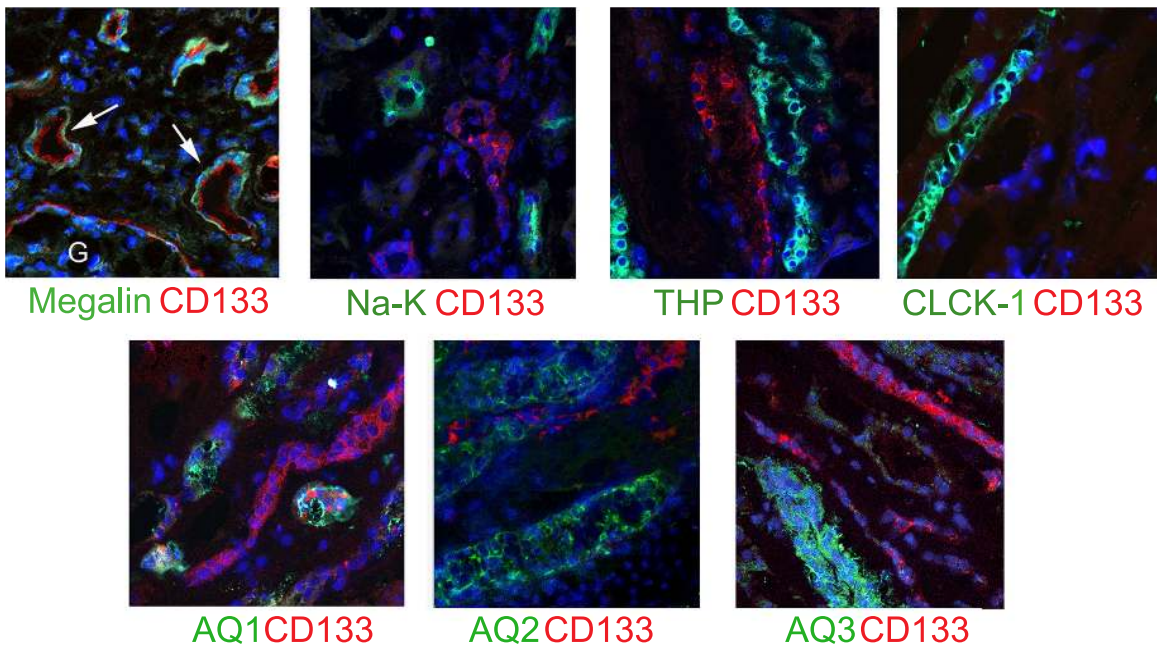


Fig. 2. Costaining of CD133+ cells and nephron markers. Representative confocal immunofluorescence micrographs showing staining of human renal tissue with CD133 (clone AC133–1; red) and specific nephron segment markers (green). Costaining was observed only for megalin in the cortical tubuli (arrows). CD133+ cells did not coexpress markers of distal tubuli (Na/Cl cotrasporter), of thin descending and thin ascending segments [aquaporin-1 (AQ1) and CLCK-1, respectively], of thick ascending segment (THP), and of collecting ducts (AQ2 and AQ3). Nuclear staining was performed with Hoechst dye 33342. Original magnification ×400. G, glomerulus.

PTL4; forward, 5′-GGC CTC TCC GTA CCC TTC TC-3′ (nt 1042–1061) and reverse, 5′-GGC CGT TGA GGT TGG AAT G-3′ (nt 1165–1147); human VEGF-A forward, 5′-TCA TCA CGA AGT GGT GAA GTT CA-3′ (nt 1146–1168) and reverse, 5′-TCA GGG TAC TCC TGG AAG ATG TC-3′ (nt 1238–1216); human TBP: forward, 5′-TGT GCA CAG GAG CCA AGA GT-3′ (nt 938–957 iso1) and reverse, 5′-ATT TTC TTG CTG CCA GTC TGG-3′ (nt 988–968 iso1) and human β-actin: forward, 5′-TGA AGA TCA AGA TCA TTG CTC CTC-3′ (nt 1058–1081) and reverse, 5′-CAC ATC TGC TGG AAG GTG GAC-3′ (nt 1151–1131).

*Cell infection and transfection.* For monitoring the transcriptional activity of Oct4, CD133+ progenitors were infected with lentiviral particles expressing the green fluorescent protein (GFP) gene under the control of the Oct4 transcriptional response element (Cignal-Lenti Oct4-reporter kit, SABiosciences, Frederick, MD), following the manufacturer's instructions. Transfection of CD133+ progenitors was performed using the HiPerFect Transfection kit (Qiagen) according to the manufacturer's protocol. For papillary CD133+ cell transfection, 50 nM miScript miRNA Mimic along with 6 μl HiPerFect Transfection Reagent (for a 24-well plate; all from Qiagen) were mixed into

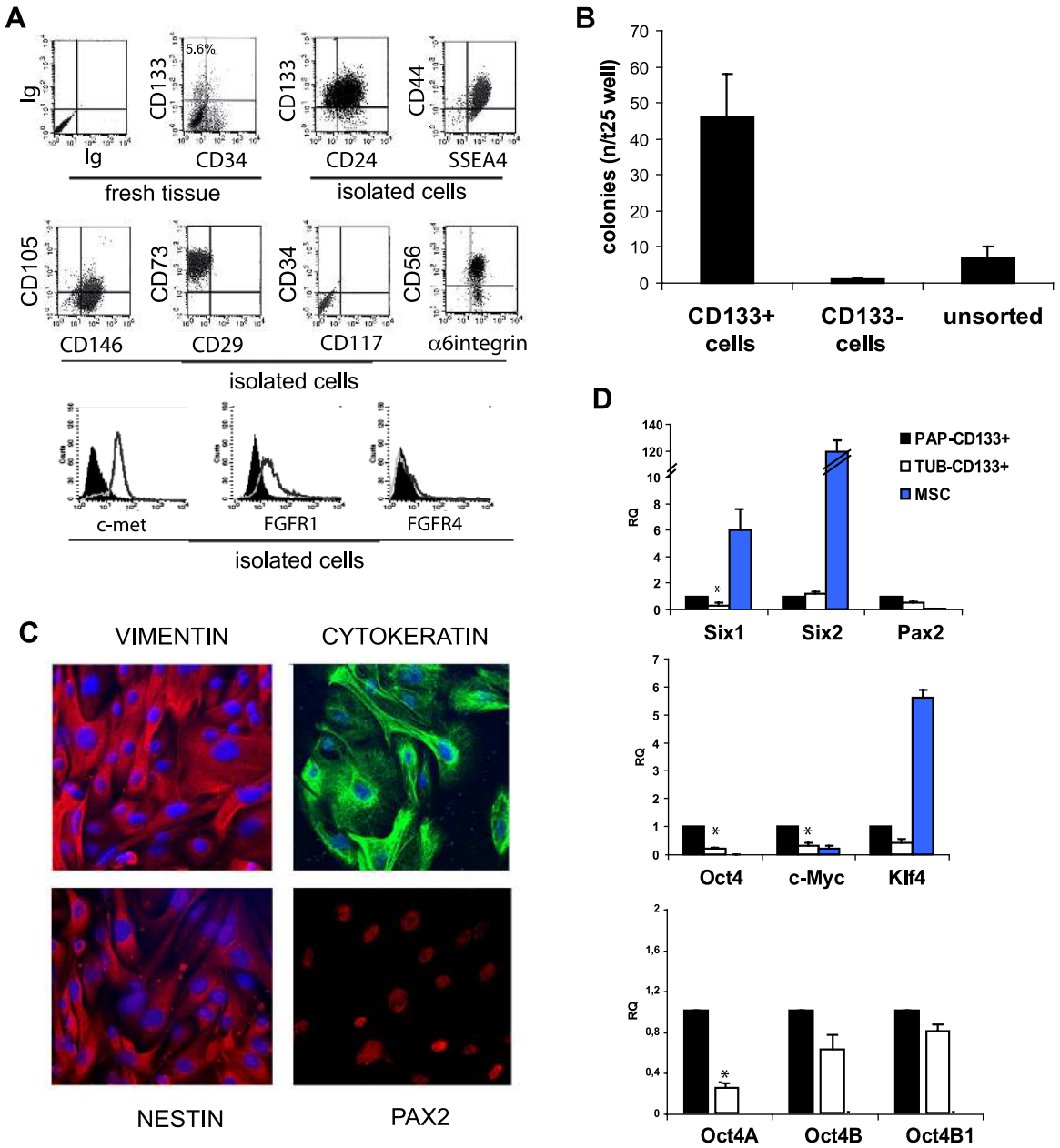


Fig. 3. Characterization of CD133+ cells. *A*: representative FACS analyses of papillary disaggregated renal tissue and of cell isolates at early culture passages. *Bottom* histograms: gray line shows binding of the specific antibody and the filled area the isotypic control. All 33 lines and 12 clones, originated from 4 different cell lines, showed similar marker expression. *B*: number of colonies originated from CD133+, CD133−, or unsorted cells. Data are means ± SD of 5 different experiments. *C*: representative micrographs of immunofluorescence staining. Nuclei were stained with Hoechst dye 33342. Original magnification ×630. All 33 lines and 12 clones, originated from 4 different cell lines, showed similar results. *D*: quantitative RT-PCR analysis of freshly isolated CD133+ cells from papillary tissue (Pap-CD133+) or cortical tubuli (Tub-CD133+) showing the expression of mRNAs encoding for the renal embryonic and stem-related factors and for the Oct4 isoforms. Mesenchymal stem cells (MSC) were used as control. All data were normalized to β-actin mRNA. The mean of 6 different cell lines was normalized to 1 for Pap-CD133. Student's *t*-test was performed. $*P < 0.05$.

500 μl of EBM without supplement kit and added to the plate. For CD133$^+$ progenitors from cortical tubuli, 10 nM Mimic or 75 nM miScript miRNA inhibitor along with 3 μl HiPerFect Transfection Reagent were used. The day after transfection, cells were washed and cultured in their expansion or differentiation media. AllStars Negative Control siRNA or miScript miRNA inhibitor (Qiagen) were used as negative control for each transfection. In all experiments, transfection was confirmed by evaluation of miR-145 levels using qRT-PCR.

*Xenograft in SCID mice.* CD133$^+$ cells, CD133$^+$ transfected cells, or clones were implanted subcutaneously into SCID mice (Charles River, Jackson Laboratories, Bar Harbor, ME) within Matrigel (Becton Dickinson), as described (2), in adherence to the Italian recommendations for the care of laboratory animals. Cells were harvested using trypsin-ethylenediaminetetraacetic acid, washed with phosphate-buffered saline, counted in a microcytometer chamber, and resuspended in DMEM ($1 \times 10^6$ in 250 μl of DMEM). Cells were chilled on ice, added to 250 μl of Matrigel at 4°C, and injected subcutaneously into the left back of SCID mice via a 26-gauge needle using a 1-ml syringe. At *day 15*, mice were killed and Matrigel plugs were recovered and analyzed.

*Statistical analysis.* Statistical analysis was performed by using the Student's *t*-test, or ANOVA with Dunnet's multicomparison tests, as appropriate. A $P$ value of $<0.05$ was considered significant.

## RESULTS

*Identification of CD133$^+$ cells in the Henle's loop and thin segments of the renal medulla.* Previous studies showed the presence of CD133$^+$ cells in the cortical region (2, 39, 40). We now systematically investigated by immunofluorescence on frozen tissue, the presence of CD133$^+$ cells within the different regions of the renal tissue (Fig. 1). As reported, in the cortex CD133$^+$ cells were detectable within the Bowman's capsule and in proximal convolutes tubules (Fig. 1, *A* and *B*). Tubular structures positive for CD133 were also present in the medulla, mainly in the human papillary region of the inner medulla, which contains thin segments of the Henle's loop and large collecting ducts (25). The CD133$^+$ structures morphologically corresponded to the Henle's loop and its thin segments (Fig. 1, *D* and *E*), whereas the ducts of Bellini in the area cribrosa were negative (Fig. 1*F*). A lower number of CD133$^+$ structures, possibly belonging to short loop nephrons, was also detectable in the outer medulla (Fig. 1*C*). Costaining with nephron segment markers showed that CD133$^+$ structures in the cortex were positive for the proximal marker megalin (10) and not for the distal marker Na/Cl cotransporter (1) (Fig. 2). Within the loop of Henle, the CD133 structures were negative both for the thin descending and for the thin ascending segment markers AQ1 (32) and CLCK-1 (43), respectively (Fig. 2). Costaining of CD133 was absent also for the thick ascending segment marker THP (38). In addition, the collecting ducts identified by staining for AQ2 and AQ3 markers (32) did not express CD133 (Fig. 2). CD133$^+$ cells detected in different regions coexpressed CD24 (Fig. 1, *inset*).

*Comparison of CD133$^+$ cells from medulla and cortex.* By cytofluorimetric analysis, the percentage of CD133$^+$ tubular cells in the papillary region of medulla ranged between 4.3 and 8.2% CD133$^+$ cells (Fig. 3*A*) and was significantly higher than that in the cortex of the same tissue specimen (means ± SE: 6.3 ± 1.6 papilla; 1.2 ± 0.4 cortex; $n = 6$, $P < 0.05$). We isolated the CD133$^+$ cells from human renal inner medulla by immunomagnetic sorting. Lines were obtained by culturing CD133$^+$ cells in complete EBM without serum at a density of $1.0 \times 10^4$ viable cells/cm$^2$. A highly enriched population containing >90% CD133$^+$ cells was obtained (Fig. 3*A*). The

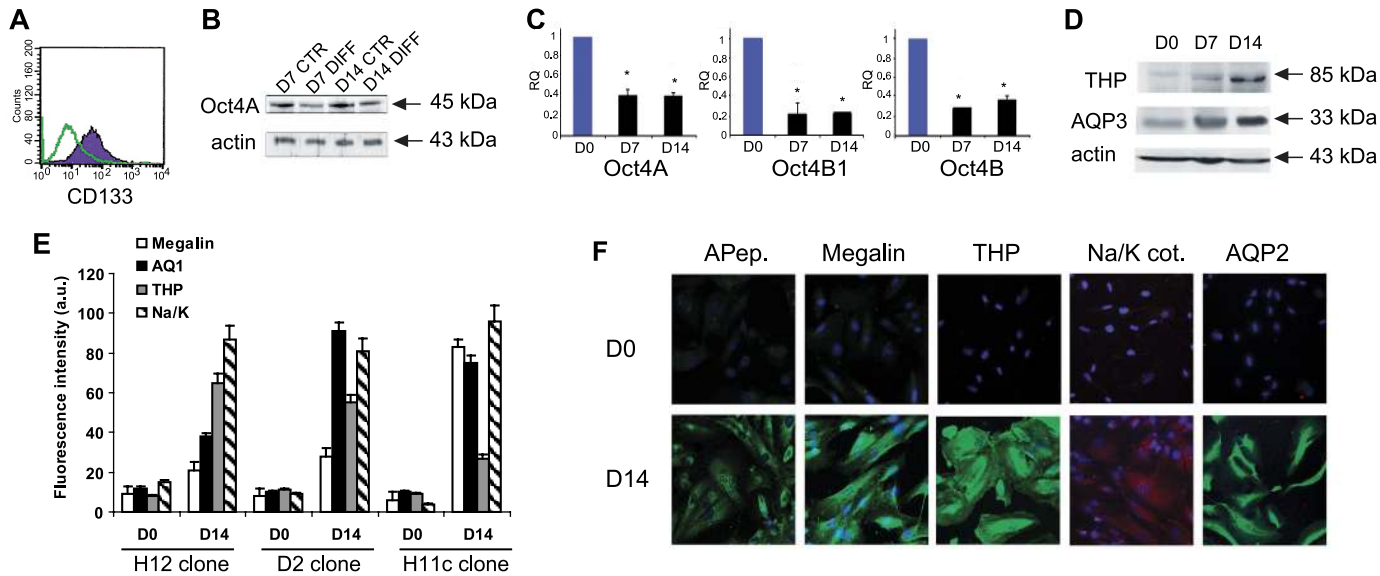


Fig. 4. Epithelial differentiation of CD133$^+$ cells from the papillary region of medulla. CD133$^+$ cells were incubated for 7 or 14 days (D7 or D14) in the presence of a differentiating epithelial medium. *A*: FACS analysis showing the loss of CD133 by differentiated cells (green line) with respect to cells cultured in the basal medium (filled area). *B*: Western blot analysis of Oct4A expression 7 or 14 days after culture in differentiation medium (DIFF) or in basal culture medium (CTR). Four different experiments were performed with similar results. *C*: quantitative RT-PCR analysis showing reduction in mRNAs encoding for the Oct4 isoforms after 7 or 14 days of differentiation. Data were normalized to TBP mRNA and to 1 for *time 0* and are means ± SD of 3 different experiments. ANOVA with Dunnett's comparison test was performed. *$P < 0.05$ vs. *time 0*. *D*: Western blot analysis showing increase of nephron markers 7 and 14 days after differentiation. Three different experiments were obtained with similar results. *E* and *F*: semiquantitative analysis of the expression of nephron markers as detected by IF staining on 3 different clones after 14 days of differentiation (*E*) and representative micrographs of the immunofluorescence staining on CD133$^+$ cells (*F*). Nuclei are stained in blue with Hoechst dye 33342. Original magnification ×630. THP, Tamm-Horsfall protein; Na/K cot, Na/K cotransporter; APep, aminopeptidase A; AQP, aquaporin.

CD133-negative fraction, confirmed by cytofluorimetric analysis to lack CD133 (not shown), did not originate colonies in the same culture conditions (Fig. 3*B*). To confirm the selection of these cells by culture conditions, culture of unsorted cells generated >90% $CD133^+$ cells (Fig. 3*A*). Cells were maintained in expansion medium without losing CD133 expression for 7 to 15 passages. Thirty-three different lines were obtained and characterized. Characterization of the initial cell isolates by fluorescence-activated cell sorting analysis showed that $CD133^+$ expressed the mesenchymal stem cell markers CD73, CD29, CD44, CD146, and the stem cell marker SSEA-4 (4). No expression of CD34, CD117, and CD45 was detected in all isolates. In addition, alpha6 integrin and CD56, a putative marker of renal progenitors expressed in the embryonic kidney (30), were positive although not in the totality of the cells (Fig. 3*A*). By immunofluorescence, $CD133^+$ cells were positive for cytokeratin, vimentin, nestin, and PAX2 (Fig. 3*C*). The pattern of markers expressed by $CD133^+$ cells derived from the papillary region of medulla was super imposable to that described for $CD133^+$ cells from the renal cortex (2).

By quantitative RT-PCR, we comparatively evaluated in $CD133^+$ progenitor cells isolated from cortex or papilla the expression of renal embryonic markers (11) and of transcription factors associated with multipotency (4) (Fig. 3*D*). All $CD133^+$ populations expressed Six1, Six2, and Pax2. Mesenchymal stem cells known to express mesenchymal transcription factors (11) but not the renal marker Pax2 (2) were used as control. In addition, both cortical and papillary CD133+ cells expressed Oct4, c-Myc, and Klf4. Indeed, the levels of these transcription factors were higher in $CD133^+$ cells from papilla. The expression of Sox2 was inconsistent among the different cell lines, being completely absent in 37% of the tested lines ($n = 8$) and highly variable in the others. We further investigated, using specific primers, the expression of the three isoforms of Oct4, that could be generated by alternative splicing, since several reports questioned the expression of the Oct4A isoform in adult stem cells (22, 45) (Fig. 3*D*). Oct4A, which is considered to associate with stemness (45), was significantly higher in $CD133^+$ derived from the papillary region of medulla in respect to those obtained from the cortical tubules. No significant differences were observed for the Oct4B isoform, associated with stress response (45), and for Oct4B1, whose role is currently unknown (Fig. 3*D*).

*In vitro differentiation.* To obtain epithelial differentiation, $CD133^+$ cells obtained from the papillary region of medulla and deriving clones were grown in the presence of growth factors known to be involved in epithelial differentiation (2).

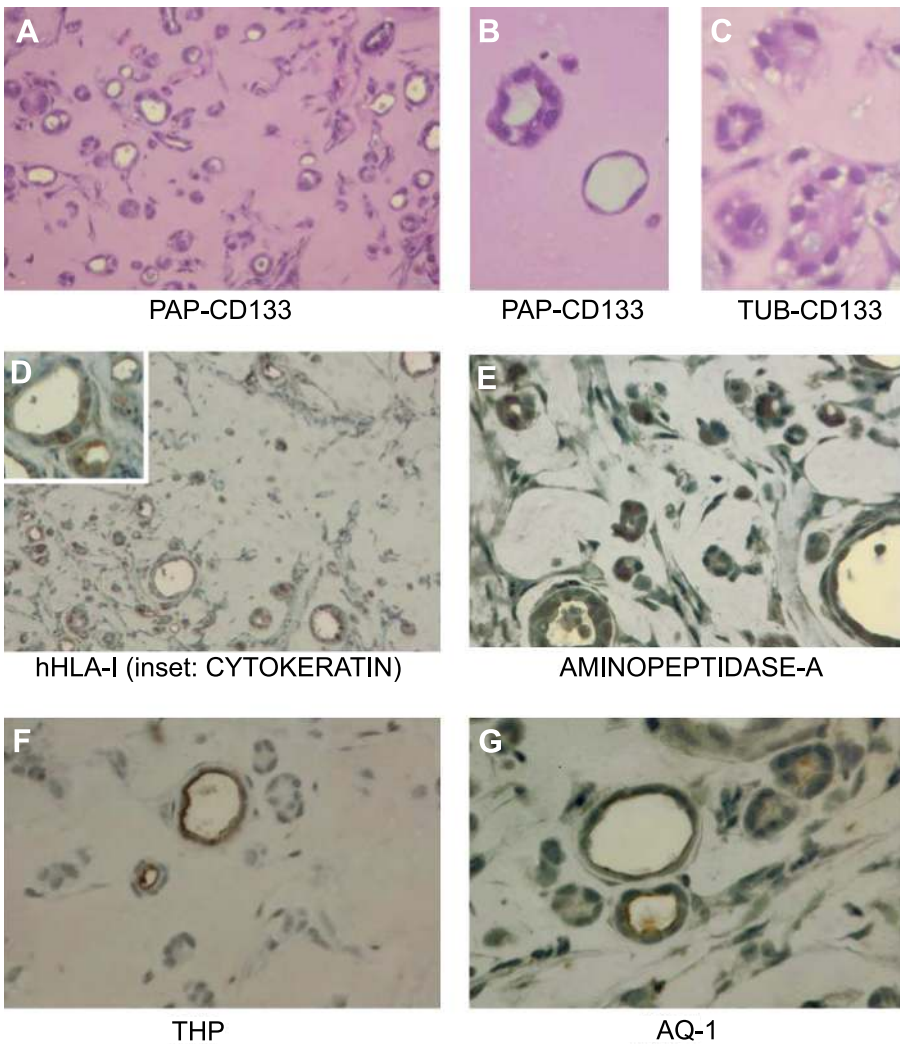


Fig. 5. In vivo differentiation of papillary $CD133^+$ cells. Undifferentiated $CD133^+$ cells ($1 \times 10^6$) were injected subcutaneously with Matrigel in SCID mice and plugs were recovered after 14 days. *A–C*: representative hematoxylin and eosin (HE) staining micrograph of tubular-like structures originated from $CD133^+$ cells. Tubular structures were covered both by cuboidal and by flat cells generated by $CD133^+$ cells from the papillary region of medulla (*B*). In contrast, $CD133^+$ from the cortex only generated cuboidal cells resembling proximal tubuli (*C*). *D–G*: immunohistochemical staining of human HLA class I (*D*), cytokeratin (*D*, *inset*), and of the different nephron segment markers aminopeptidase A (*E*), THP (*F*), and AQ1 (*G*). Magnification *A*, *D*: ×250; *B*, *C*, *E–G*, and *D*, *inset*: ×400. Five different cell lines and 3 clones were analyzed with similar results.

As CD133$^+$ cells expressed the HGF receptor c-met and the FGF-4 receptor FGFR1, but they did not express FGFR4, receptor for other FGF isoforms, we cultured them for 14 days in medium containing HGF and FGF4 (Fig. 3*A*). After culture in differentiating conditions, cells lost CD133$^+$ expression and downregulated Oct4A expression (Fig. 4, *A* and *B*). The downregulation of the mRNA level of the three Oct4 isoforms was confirmed by quantitative RT-PCR (Fig. 4*C*). In parallel, after culture in epithelial differentiating condition, CD133$^+$ cells and clones acquired markers characteristic of fully differentiated renal epithelia, such as megalin and amino peptidase A, mainly expressed by proximal tubular epithelial cells (10, 29), THP, expressed by the thick limb of the Henle's loop (38), the thiazide-sensitive NaCl cotransporter, mainly expressed by distal tubular epithelial cells (1), AQ1, expressed by distal tubules and thin descending limbs and AQ2 and AQ3 expressed by collecting ducts (32) (Fig. 4, *D–F*). This differentiation ability was similar to that reported in vitro for CD133$^+$ cells from cortical tubules (2).

*In vivo differentiation.* CD133$^+$ cells were subcutaneously injected into Matrigel in SCID mice to assess their differentiation in vivo. After 10–15 days, plugs were recovered and processed for histological and immunohistochemical analysis. Undifferentiated cells injected into mice showed a spontaneous differentiation into epithelial tubular structure with aspects of cuboidal or flat epithelium (Fig. 5, *A* and *B*). Immunohistochemical evaluation indicated that these structures were human, as they expressed HLA class I antigen, and were positive for the epithelial marker cytokeratin as well as for markers of the different nephron segments: proximal tubular marker amino peptidase A, Henle's loop markers THP and AQ1, selective for the thick and for the thin descending segments, respectively (Fig. 5, *D–G*). At variance, renal cortex CD133$^+$ cells only differentiated into cuboidal structures resembling proximal tubuli (Fig. 5*C*). Injec-

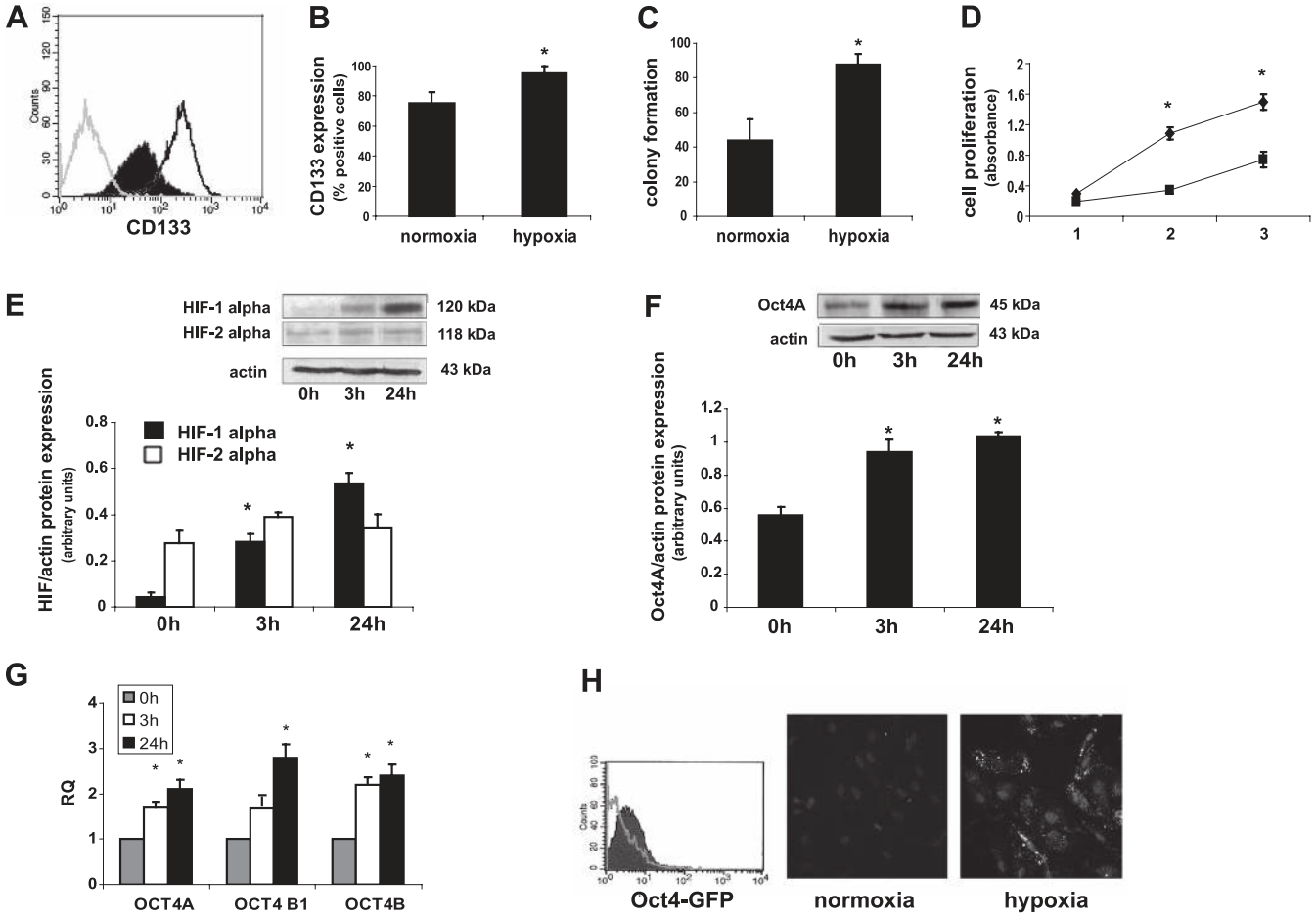


Fig. 6. Effect of hypoxia on CD133$^+$ cells from the papillary region of medulla. *A*: representative cytofluorimetric analysis of CD133$^+$ expression in normoxia (filled area) or after 24-h hypoxia (dark line). The gray line shows the isotypic control. *B*: quantification of the percentage of CD133$^+$ cells in 6 different preparations evaluated by cytofluorimetric analysis in normoxia or after 72-h hypoxia (1% $O_2$). *C*: evaluation of the generation of single-cell derived colonies, as described in METHODS, by CD133$^+$ cells in normoxia or hypoxia. *D*: evaluation of cell proliferation by BrdU incorporation in hypoxia (▲) in respect to normoxia (■). *B–D*: values are means ± SD of 6 different experiments performed in triplicate. Student's *t*-test was performed. *$P < 0.05$ normoxia vs. hypoxia. *E*, *F*: Western blot micrograph and densitometric analysis of HIF-1α and HIF-2α (*E*) and of Oct4A (*F*) expression in cells at *time 0* or after 3- and 24-h hypoxia. Data, shown as arbitrary units, are representative of 6 different experiments and were normalized to actin expression. *G*: quantitative RT-PCR analysis showing the variation of Oct4 isoforms induced by hypoxia. Data were normalized to TBP mRNA and to 1 for *time 0*. Data are means ± SD of 3 different experiments. *E–G*: ANOVA with Dunnett's comparison test was performed. *$P < 0.05$ vs. *time 0*. *H*: increase in Oct4 promoter activity after 48-h hypoxia in CD133$^+$ cells infected with a GFP-Oct4 promoter vector. Increase in GFP expression was showed by cytofluorimetric analysis in cells under hypoxia (filled line) with respect to cells in normoxia (gray line) and by immunofluorescence analysis by representative micrographs in cells 48 h after hypoxia with respect to normoxia. Original magnification ×400.

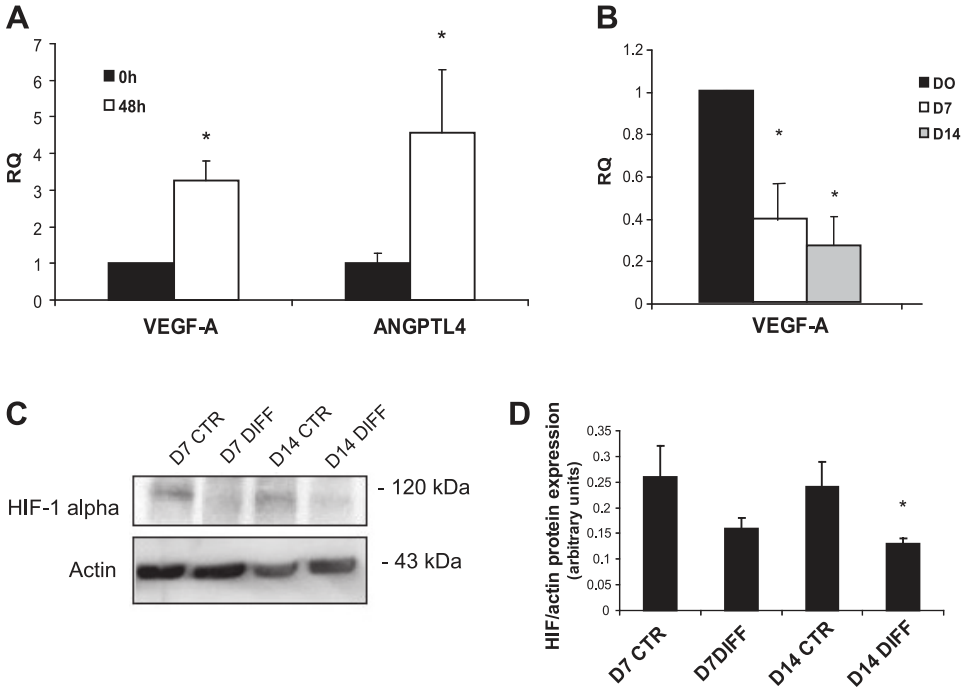


Fig. 7. Vascular endothelial growth factor (VEGF) synthesis by undifferentiated and differentiated cells. *A*: quantitative RT-PCR analysis showing the increase in VEGF and ANGPL4 induced by 48-h hypoxia in papillary CD133+ cells. Data were normalized to TBP mRNA and to 1 for normoxia. Data are means ± SD of 3 different experiments. Student's *t*-test was performed. *$P < 0.001$ normoxia vs. hypoxia. *B*: quantitative RT-PCR analysis showing the variation of VEGF in CD133+ cells after 7 or 14 days of epithelial differentiation. Data were normalized to TBP mRNA and to 1 for normoxia. Data are means ± SD of 3 different experiments. Student's *t*-test was performed. *$P < 0.001$ *day 0* vs. *day 7* or *day 14*. *C–D*: Western blot micrograph and densitometric analysis of HIF-1α expression in cells after culture for 7 or 14 days in differentiation medium (DIFF) or in basal culture medium (CTR). Data, shown as arbitrary units, are mean of 3 different experiments and were normalized to actin expression. Student's *t*-test was performed. *$P < 0.05$ DIFF vs. CTR.

tion of CD133+ papillary progenitors from single clones ($n = 3$) generated similar tubular structures (not shown).

*Hypoxia modulates stem cell properties of CD133+ cells derived from the papillary region of medulla.* The papillary region of the medulla has a very low-oxygen tension, ranging ~10 mmHg, whereas the cortex benefits from an oxygen tension between 30 and 50 mmHg (15). We therefore evaluated whether hypoxia may modulate the undifferentiated phenotype of CD133+ progenitors. When CD133+ cells were cultured under hypoxia in 1% oxygen, corresponding to an oxygen tension of 10 mmHg (8), the expression of CD133 was upregulated as soon as after 24 h and maintained up to 72 h (Fig. 6, *A* and *B*). In parallel, culture in hypoxic condition significantly promoted CD133+ cell proliferation and the ability to form colonies from a single cell, that showed a twofold increase (Fig. 3, *C* and *D*), suggesting that hypoxia may modulate the progenitor/stem phenotype. We also evaluated the activation of the hypoxia-inducible factors HIF1α and HIF2α, master regulators of the transcription effect of hypoxia (16). Hypoxia promoted a rapid upregulation of HIF1α, whereas HIF2α, which was constitutively expressed in CD133+ cells, did not increase after hypoxic exposure (Fig. 6*E*). Moreover, hypoxia enhanced the expression of Oct4 protein (Fig. 6*F*). However, levels expressed by CD133+ cells derived from the papillary region of medulla were significantly lower than those in murine embryonic stem cells used as control (not shown). In addition, we found that the mRNA levels of the three Oct4 isoforms were upregulated by hypoxia as soon as 3 h (Fig. 6*G*). The effect was maintained up to 24 h (Fig. 6*G*) and 48 h (not shown). Increase in angiopoietin-like4, a potent angiogenic factor known to be regulated by hypoxia (20), was used as control of cell activation by hypoxia (positive response → 2-fold increase in angiopoietin-like4 mRNA normalized to TBP mRNA). To validate the effect of hypoxia on Oct4 synthesis, we infected CD133+ cells with an Oct4-responsive GFP vector. After 48-h hypoxia, infected cells expressed GFP, evaluated by cytofluorimetric analysis and immunofluorescence, indicating the activation of the Oct4 transcription (Fig. 6*H*). No effect of hypoxia was observed on Nanog, c-Myc, or Klf4 by quantitative RT-PCR (not shown). Hypoxia (24–72 h) did not modulate the transcription factors Snail, Slug, and Twist (not shown), involved in the epithelial-mesenchymal transition (31). In addition, hypoxia promoted the synthesis of VEGF, known to be a target of the transcriptional activity of HIF-1 (Fig. 7*A*). VEGF was in turn reduced during differentiation of CD133+ cells from papilla, in concomitance with a reduction of HIF-1 alpha levels (Fig. 7, *B–D*).

*MiR-145 modulates CD133+ cell properties.* To investigate the possible mechanism of Oct4 regulation in CD133+ cells, we evaluated the involvement of miR-145, known to repress Oct4 synthesis in human embryonic stem cells (6, 47). We found that CD133+ cells from papilla constitutively expressed miR-145, which was downregulated during hypoxia (Fig. 8*A*). Conversely, miR-145 levels increased during cell differentiation, concomitantly with the downregulation of Oct4. In particular, miR-145 levels showed a peak at *day 7* after differentiation. After 14 days of differentiation, miR-145 levels were significantly higher than at *time 0* (Fig. 8*B*), although they decreased in respect to *day 7* possibly due to inhibitory mechanisms activated once cells reached a complete differentiation. Indeed, MiR-145 levels were higher in mature CD133− cells obtained from fresh tissue than in CD133+ cells (Fig. 8*B*). To investigate the causative effect of miR-145 on Oct4 downregulation, we generated CD133+ cells expressing high levels of miR-145 by transfection with a miR-145 mimic (Mimic145) (Fig. 8*C*). As control, cells were transfected with Allstar negative control (CTR-A). The levels Oct4A protein were significantly reduced in Mimic 145 cells in respect to CTR-A cells (Fig. 8*D*), but not its mRNA (not shown), suggesting an effect of miR-145 at the translation level. No difference in the expression of the Oct4B isoform was observed in Mimic 145 cells (not shown). In parallel, overexpression of miR-145

induced a reduction in cell proliferation rate (Fig. 8*E*). Moreover, Mimic145 cells, cultured in the presence of epithelial differentiating medium, showed an increase in differentiation ability as soon as *day 3*, evaluated as acquisition of specific tubular markers by immunofluorescence staining in respect to CTR-A or nontransfected cells (Fig. 8*F*). In vivo, Mimic145 cells lost the ability to form tubular structures when injected into Matrigel in SCID mice (Fig. 8*G*), as isolated mature CD133$^-$ cells.

*Effect of hypoxia on tubular CD133$^+$ cells.* We also evaluated whether the effect of hypoxia on maintenance of progenitor properties was unique to papillary CD133$^+$ by studying

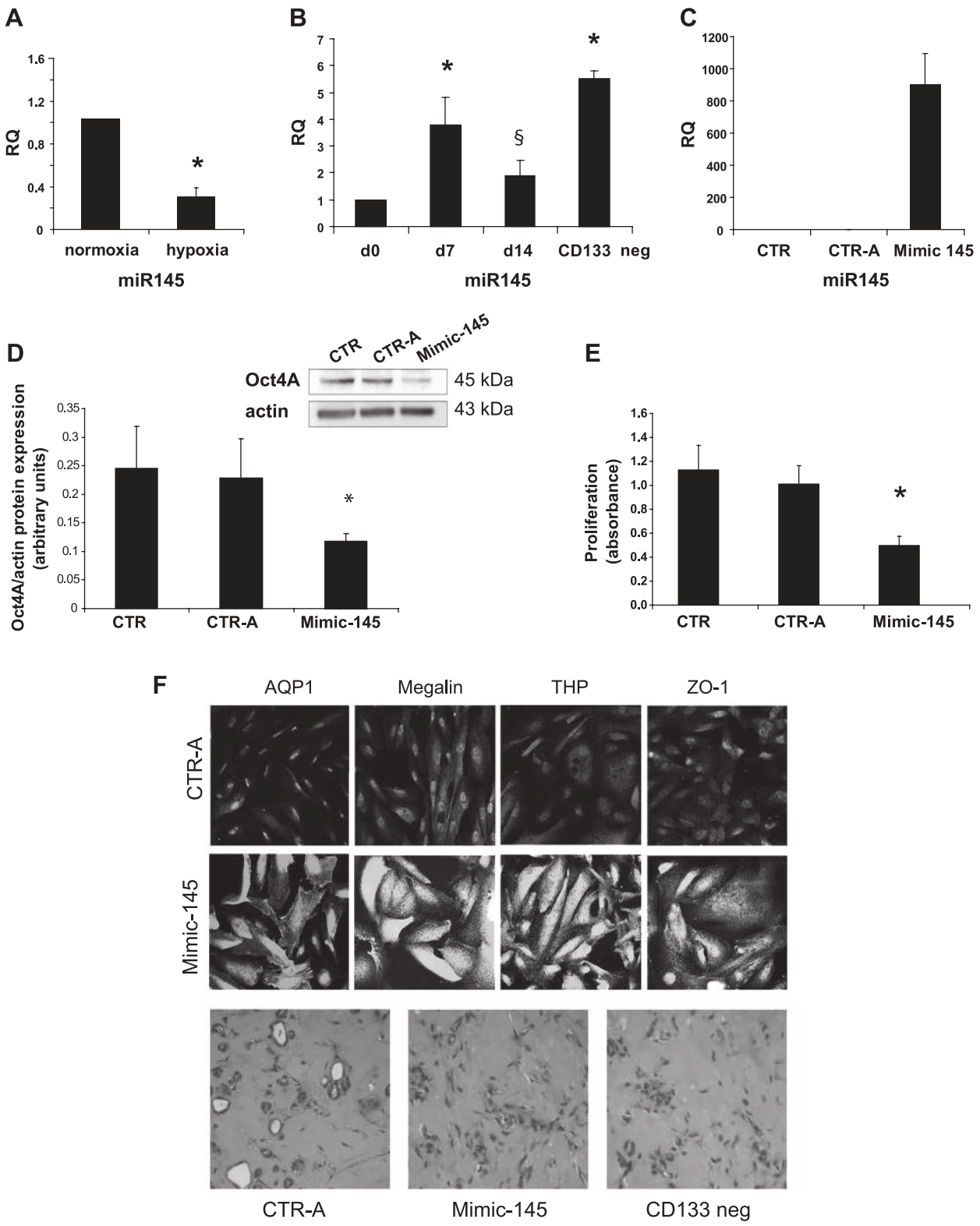

cortical tubular CD133+ cells. We found that hypoxia increased CD133 expression in tubular CD133$^+$ cells (Fig. 9*A*). In addition, hypoxia promoted VEGF and ANGPLF4 expression, showing similar functional effects to papillary CD133$^+$ (Fig. 9*B*). We therefore investigated the effect of hypoxia on Oct4 expression. Tubular CD133$^+$ cells showed in basal culture condition low Oct4A levels in respect to papillary CD133$^+$ cells both at RNA (Fig. 3*D*) and at protein level (Fig. 9*C*). Conversely, the Oct4B isoform, known to be associated with the stress response, was increased at protein level in tubular CD133$^+$ cells (Fig. 9*C*). After 24 h hypoxia, Oct4 mRNA expression was increased in all the three isoforms (Fig. 9*D*). However, possibly due to the low levels, Oct4A protein remained undetectable even after hypoxia, whereas the Oct4B isoform was increased (Fig. 9, *E* and *F*). At variance, papillary CD133$^+$ showed a prevalent increase in Oct4A isoform, whereas the Oct4B isoform was almost undetectable (Fig. 9*E*). We also investigated the possible role of miR-145 in the regulation of Oct4 in cortical tubular CD133$^+$ cells. Tubular CD133$^+$ cells showed basal miR-145 levels similar to those observed in papillary CD133$^+$ cells (not shown). We therefore modulated miR-145 levels by generating CD133$^+$ cells expressing high levels of miR-145 (Mimic145) or we inhibited miR-145 using a miRNA inhibitor (anti-MiR145). As shown in Fig. 9, *G* and *H*, miR-145 regulated Oct4B but not Oct4A isoform. Increase in miR-145 levels in Mimic-145 cells decreased Oct4B (Fig. 9, *G* and *H*). Conversely, inhibition of miR-145 activity in anti-MiR145 cells increased Oct4B levels (Fig. 9, *G* and *H*). No effect was observed on Oct4A isoform. Altogether, these data suggest a major role for activation of the stress response in tubular CD133$^+$ cells by hypoxia.

## DISCUSSION

In the present study, we found that CD133$^+$ progenitor cells are present in different segments of the nephron. In particular, they were enriched in the Henle's loop and thin segments in the papillary region of medulla. Once isolated, the CD133$^+$ cells derived from the papillary region of medulla expressed transcription factors associated with stemness and the ability to generate in vivo canalized structures positive for renal specific markers. These cells showed Oct4 levels and differentiation potential higher than those obtained from cortical tubuli. In addition, we found that hypoxia was able to modulate the phenotype of CD133$^+$ progenitors, enhancing the ability to form colonies, stimulating the expression of CD133 and the synthesis of the Oct4. Moreover, we provided evidence that miR-145 may induce Oct4 regulation during hypoxia and differentiation.

This finding in the human kidney is consistent with the previous observation by Oliver et al. (33, 34) that the papilla may represent a preferential site of localization of stem/progenitor cells. CD133$^+$ cells were present in the Henle's loop and its thin limb segments, and they did not coexpress nephron markers. At variance, the papillary stem cells in rodents were located in collecting duct cells or interstitial cells, and not in the Henle's loop. This could be due to an anatomical difference of human kidney that presents multiple papillas and a less defined papillary region than that of mice that is unipapillate (25). The localization of CD133$^+$ cells within the different segments of the nephron in humans may suggest that this population is not confined in a specific niche and that it may modulate its phenotype in response to the microenvironmental factors. However, CD133$^+$ cells in the papillary region were more abundant than in the cortex and they were negative for segment-specific nephron markers at variance of the tubular CD133$^+$ cells in the cortex. Moreover, they expressed embryonic transcription factors and they were enriched in Oct4A in respect to tubular CD133$^+$ cells, which expressed preferentially the Oct4B isoform involved in the stress response. These results may suggest that the papilla and in particular the Henle's loop may represent an environment that favors the maintenance of undifferentiated phenotype of epithelial precursors. This is consistent with the report that Oct4-positive cells reside in the papilla in rodents (21). The relatively high number of the cells as well as their constitutive expression of the epithelial marker cytokeratin define this population as epithelial progenitors. Indeed, in the human fetal kidney, CD133$^+$/CD24$^+$ cells represent >50% of the population and express epithelial surface markers (39). The nature of CD133$^+$ cells as epithelial progenitors is also confirmed by our in vivo experiments where the undifferentiated CD133$^+$ cells spontaneously generated epithelial tubular-like structures. Of interest, CD133$^+$ from the papillary region of medulla, at variance of those obtained by the tubular cortex, showed the ability to generate tubular-like structures with variable morphology and with the expression of markers of different nephron segments. Altogether, these data may indicate the presence of populations of cells with a different degree of differentiative commitment within the nephron and suggest a role for the hypoxia microenvironment of the papilla in the progenitor properties of CD133$^+$ cells.

Fig. 8. Role of miR-145 in the differentiation of CD133$^+$ cells from the papillary region of medulla. *A*: evaluation of miR-145 levels by quantitative RT-PCR in CD133$^+$ cells after 24-h hypoxia. RNA imputs were normalized to RNU48 and to 1 for normoxia. Data are means ± SD of 3 different experiments. Student's *t*-test was performed. *$P < 0.05$ vs. normoxia. *B*: evaluation of miR-145 levels by quantitative RT-PCR in CD133$^+$ cells, after culture for 0, 7, or 14 days in epithelial differentiating medium, or in CD133$^-$ cells. RNA imputs were normalized to RNU48 and to 1 for *time 0*. Data are means ± SD of 6 different experiments. Student's *t*-test was performed. *$P < 0.001$, §$P < 0.05$ vs. *d0*. *C*: MiR-145 levels in CD133$^+$ cells (CTR), in cells transfected with Allstar negative control (CTR-A) or with a miR-145 mimic (Mimic 145). RNA imputs were normalized to RNU48. *D*: Western blot micrograph and densitometric analysis of Oct4A expression in CTR or CTR-A or Mimic145 cells. Data were normalized to actin expression and are shown as arbitrary units. ANOVA with Dunnett's comparison test was performed. *$P < 0.05$ Mimic145 vs. CTR or CTR-A. *E*: cell proliferation by BrdU incorporation. Values are means ± SD of 4 different experiments performed in triplicate. ANOVA with Dunnett's comparison test was performed. *$P < 0.05$ Mimic145 vs. CTR or CTR-A. *F*: representative micrographs showing the immunofluorescence staining for nephron markers by Mimic 145 cells with respect to CTR-A cells after 3 days of culture in epithelial differentiating medium. Nuclei were stained with Hoechst dye 33342. Original magnification ×630. *G*: representative HE staining micrograph of tubular-like structures formed in vivo by Mimic145, CTR-A cells, and CD133$^-$ cells in Matrigel when injected in SCID mice. Original magnification ×250. Eight different experiments were performed with similar results.

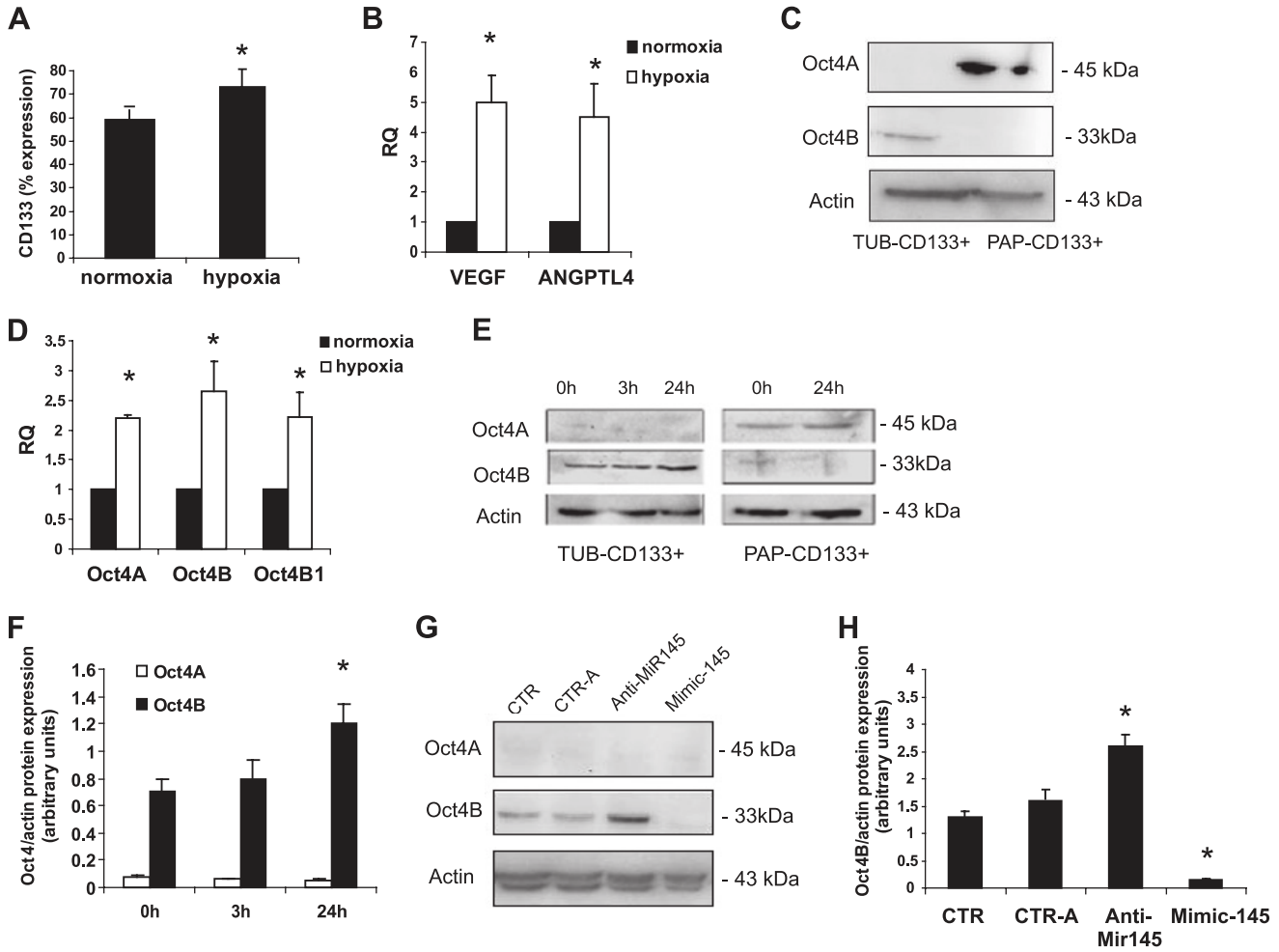


Fig. 9. Effect of hypoxia on tubular CD133$^+$ cells from the renal cortex. *A*: effect of 24-h hypoxia (1% $O_2$) on the percentage of CD133$^+$ cells evaluated by cytofluorimetric analysis. Values are means ± SD of 3 different experiments performed in different cell preparations. *B*: quantitative RT-PCR analysis showing the increase in VEGF and ANGPL4 induced by hypoxia in tubular CD133$^+$ cells. Data were normalized to TBP mRNA and to 1 for normoxia. Data are mean of 3 different experiments. *C*: Western blot analysis of Oct4 expression in CD133$^+$ cells from cortex or papilla showing the expression of Oct4B in tubular cortical CD133$^+$ cells (TUB-CD133$^+$) and of Oct4A in papillary CD133$^+$ cells (PAP-CD133$^+$). *D*: quantitative RT-PCR analysis showing the variation of Oct4 isoforms induced by hypoxia in tubular CD133$^+$ cells. Data were normalized to TBP mRNA and to 1 for normoxia. Data are means ± SD of 3 different experiments. *B–D*: Student's *t*-test was performed. *$P < 0.05$ normoxia vs. hypoxia. *E–F*: Western blot micrograph and densitometric analysis of Oct4A and Oct4B expression in tubular CD133$^+$ cells at *time 0* or after 3- or 24-h hypoxia. Data, shown as arbitrary units, are representative of 3 different experiments and were normalized to actin expression. Oct4 isoforms in lysates of papillary CD133$^+$ cells at 0 and 24 h of hypoxia, analyzed in the same blot of tubular CD133$^+$ cells, were used as control (*E*). *G–H*: Western blot micrograph and densitometric analysis of Oct4A and Oct4B expression in tubular in CD133$^+$ cells (CTR), in cells transfected with Allstar negative control (CTR-A), or with a miR-145 mimic (Mimic145) or with an anti-miR145 antisence (Anti-miR145). Data, shown as arbitrary units, are representative of 3 different experiments and were normalized to actin expression. *F* and *H*: ANOVA with Dunnett's comparison test was performed. *$P < 0.05$ vs. *time 0* or CTR.

$O_2$ has been shown to regulate death and differentiation of embryonic stem cells and adult progenitors (35, 41). Low-oxygen tension is an important component of the stem cell microenvironment and niche and provides signals conducive to the maintenance of definitive stem cell properties (41). Previous studies showed that hypoxia increased CD133 through HIF-1α in neural progenitors and glioma stem cells (36, 42). We found that hypoxia enhanced the number of CD133$^+$ cells and promoted their proliferation and ability to generate colonies, indicating a role in their stem-related phenotype. Another property of hypoxia is the activation of specific pathways and transcription factors that control stem cells, such as Oct4. HIF-2α was reported to bind to the Oct-4 promoter and to induce Oct-4 expression in embryonic stem cells (9). An increase in Oct4 mRNA after hypoxia exposure was also observed in mesenchymal stem cells (14). In the present study, we showed that hypoxia promoted the synthesis of the Oct4 isoforms, possibly via HIF-1α activation whose levels increased after hypoxia. Interestingly, HIF-1α decreased after differentiation, suggesting a possible hypoxia-independent modulation of HIF-1α in the maintenance of stemness, as recently shown in cancer stem cells (46).

An additional mechanism involved in stemness during hypoxia was the downregulation of miR-145. In turn, miR-145 was found to inhibit Oct4A protein synthesis, but not Oct4 mRNA levels, indicating a posttranslational mechanism involved in the phenotype of CD133$^+$ cells. Moreover, miR-145 overexpression inhibited proliferation and organization in vivo into tubular structures and stimulated downregulation of stem cell markers and differentiation. Indeed, miRNA-145 has been

proposed as a mechanism of epigenic modulation of proliferative and differentiative properties (28, 47). A miR-145 reduction was shown in undifferentiated renal tumors in respect to normal renal tissue (13). In embryonic stem cells, miR-145 inhibited Oct4 protein expression. In turn, Oct4 repressed miR-145 transcription implying a reciprocal regulation in stem cell pluripotency (6, 47). In adult cells, the possible role of Oct4 expression is still uncertain and it might be related to self renewal (19). We here found that CD133$^+$ progenitors express low-Oct4 levels and not other pluripotency genes such as Sox-2. In this context, miR-145 reduction in CD133$^+$ cells during hypoxia, possibly through activation of Oct4, may allow cell proliferation and maintenance of a progenitor phenotype. At variance, miRNA-145 upregulation and Oct4 reduction during differentiation may allow cell maturation and stop proliferation. As the effect of miR-145 was shown only on Oct4 protein synthesis and not on mRNA expression, it may be suggested that mechanisms other than miR145 may regulate Oct4 at mRNA level and contribute to maintain low Oct4 in differentiated cells.

The role of Oct4/miR145 balance in response to hypoxia was also investigated in cortical tubular CD133$^+$ cells. The results showed that hypoxia increased CD133 expression and release of proangiogenic factors. However, the response of tubular CD133$^+$ cells was related to Oct4B and not to Oct4A isoform activation, indicating a major role for the activation of the stress response in tubular CD133$^+$ cells by hypoxia. Therefore, in renal injury, hypoxia may play a role in modulating resident progenitor cells in tubuli by activating a stress response. Indeed, it has been shown that the ischemic injury may enhance the number of CD133$^+$ cells within the kidney (24).

In conclusion, we found that progenitor cells located within the nephron can be modulated by hypoxia toward an immature phenotype through a balance between Oct4 expression and miR-145 downregulation. This mechanism may be at the basis of the maintenance of a CD133$^+$ population in the papillary region of the human inner medulla. Fine-tuning of the Oct4/miR-145 balance may regulate proliferation and differentiation after injury.

## GRANTS

This work was supported by Italian Ministry of University and Research PRIN08 and ex60%, and by Regione Piemonte, PISTEM.

## DISCLOSURES

No conflicts of interest, financial or otherwise, are declared by the author(s).

## AUTHOR CONTRIBUTIONS

Author contributions: B.B. conception and design of research; B.B., A.M., F.C., G.A., G.D., and C.G. performed experiments; B.B., A.M., F.C., and C.G. analyzed data; B.B., F.C., and G.C. interpreted results of experiments; B.B. and G.C. prepared figures; B.B. drafted manuscript; B.B. and G.C. edited and revised manuscript; B.B., A.M., F.C., G.A., G.D., C.G., and G.C. approved final version of manuscript.

## REFERENCES

1. **Biner HL, Arpin-Bott MP, Loffing J, Wang X, Knepper M, Hebert SC, Kaissling B.** Human cortical distal nephron: distribution of electrolyte and water transport pathways. *J Am Soc Nephrol* 13: 836–847, 2002.
2. **Bussolati B, Bruno S, Grange C, Buttiglieri S, Deregibus MC, Cantino D, Camussi G.** Isolation of renal progenitor cells from adult human kidney. *Am J Pathol* 166: 545–555, 2005.
3. **Cantaluppi V, Biancone L, Romanazzi GM, Figliolini F, Beltramo S, Ninniri MS, Galimi F, Romagnoli R, Franchello A, Salizzoni M, Perin PC, Ricordi C, Segoloni GP, Camussi G.** Loss of nephrin expression in glomeruli of kidney-transplanted patients under m-TOR inhibitor therapy. *Am J Transplant* 10: 2270–2278, 2010.
4. **Chamberlain G, Fox J, Ashton B, Middleton J.** Concise review: mesenchymal stem cells: their phenotype, differentiation capacity, immunological features, and potential for homing. *Stem Cells* 25: 2739–2749, 2007.
5. **Chambers I, Tomlinson SR.** The transcriptional foundation of pluripotency. *Development* 136: 2311–2322, 2009.
6. **Chivukula RR, Mendell JT.** Abate and switch: miR-145 in stem cell differentiation. *Cell* 137: 606–608, 2009.
7. **Collino F, Deregibus MC, Bruno S, Sterpone L, Aghemo G, Viltono L, Tetta C, Camussi G.** Microvesicles derived from adult human bone marrow and tissue specific mesenchymal stem cells shuttle selected pattern of miRNAs. *PLos One* 5: e11803, 2010.
8. **Conforti L, Petrovic M, Mohammad D, Lee S, Ma Q, Barone S, Filipovich AH.** Hypoxia regulates expression and activity of Kv1.3 channels in T lymphocytes: a possible role in T cell proliferation. *J Immunol* 170: 695–702, 2003.
9. **Covello KL, Kehler J, Yu H, Gordan JD, Arsham AM, Hu CJ, Labosky PA, Simon MC, Keith B.** HIF-2alpha regulates Oct-4: effects of hypoxia on stem cell function, embryonic development, and tumor growth. *Genes Dev* 20: 557–570, 2006.
10. **Cui S, Verroust PJ, Moestrup SK, Christensen EI.** Megalin/gp330 mediates uptake of albumin in renal proximal tubule. *Am J Physiol Renal Fluid Electrolyte Physiol* 271: F900–F907, 1996.
11. **Dressler GR.** Advances in early kidney specification, development and patterning. *Development* 136: 3863–3874, 2009.
12. **Duffield JS, Humphreys BD.** Origin of new cells in the adult kidney: results from genetic labeling techniques. *Kidney Int* 79: 494–501, 2011.
13. **Gan B, Lim C, Chu G, Hua S, Ding Z, Collins M, Hu J, Jiang S, Fletcher-Sananikone E, Zhuang L, Chang M, Zheng H, Wang YA, Kwiatkowski DJ, Kaelin WG Jr, Signoretti S, DePinho RA.** FoxOs enforce a progression checkpoint to constrain mTORC1-activated renal tumorigenesis. *Cancer Cell* 18: 472–484, 2010.
14. **Grayson WL, Zhao F, Bunnell B, Ma T.** Hypoxia enhances proliferation and tissue formation of human mesenchymal stem cells. *Biochem Biophys Res Commun* 358: 948–953, 2007.
15. **Gunaratnam L, Bonventre JV.** HIF in kidney disease and development. *J Am Soc Nephrol* 20: 1877–1887, 2009.
16. **Guo JK, Cantley LG.** Cellular maintenance and repair of the kidney. *Annu Rev Physiol* 72: 357–376, 2010.
17. **Humphreys BD, Valerius MT, Kobayashi A, Mugford JW, Soeung S, Duffield JS, McMahon AP, Bonventre JV.** Intrinsic epithelial cells repair the kidney after injury. *Cell Stem Cell* 6: 284–291, 2008.
18. **Jászai J, Farkas LM, Fargeas CA, Janich P, Haase M, Huttner WB, Corbeil D.** Prominin-2 is a novel marker of distal tubules and collecting ducts of the human and murine kidney. *Histochem Cell Biol* 133: 527–539, 2010.
19. **Kristensen DM, Nielsen JE, Kalisz M, Dalgaard MD, Audouze K, Larsen ME, Jacobsen GK, Horn T, Brunak S, Skakkebaek NE, Leffers H.** OCT4 and downstream factors are expressed in human somatic urogenital epithelia and in culture of epididymal spheres. *Mol Hum Reprod* 16: 835–845, 2010.
20. **Le Jan S, Amy C, Cazes A, Monnot C, Lamandé N, Favier J, Philippe J, Sibony M, Gasc JM, Corvol P, Germain S.** Angiopoietin-like 4 is a proangiogenic factor produced during ischemia and in conventional renal cell carcinoma. *Am J Pathol* 162: 1521–1528, 2003.
21. **Lee PT, Lin HH, Jiang ST, Lu PJ, Chou KJ, Fang HC, Chiou YY, Tang MJ.** Mouse kidney progenitor cells accelerate renal regeneration and prolong survival after ischemic injury. *Stem Cells* 28: 573–584, 2010.
22. **Liedtke S, Stephan M, Kögler G.** Oct4 expression revisited: potential pitfalls for data misinterpretation in stem cell research. *Biol Chem* 389: 845–850, 2008.
23. **Little MH.** Tracing the life of the kidney tubule- re-establishing dogma and redirecting the options. *Cell Stem Cell* 2: 191–192, 2008.
24. **Loverre A, Capobianco C, Ditonno P, Battaglia M, Grandaliano G, Schena FP.** Increase of proliferating renal progenitor cells in acute tubular necrosis underlying delayed graft function. *Transplantation* 85: 1112–1119, 2008.
25. **Madsen KM, Nielsen S, Tisher CC.** The anatomy of the kidney. In: *The Kidney*, 8th ed., edited by Brenner BM and Rector FC Jr. Philadelphia: WB Saunders, 1997, p. 25–76.
26. **Maeshima A, Sakurai H, Nigam SK.** Adult kidney tubular cell population showing phenotypic plasticity, tubulogenic capacity, and integration capability into developing kidney. *J Am Soc Nephrol* 17: 188–198, 2006.

27. **Maeshima A, Yamashita S, Nojima Y.** Identification of renal progenitor-like tubular cells that participate in the regeneration processes of the kidney. *J Am Soc Nephrol* 14: 3138–3146, 2003.
28. **Mallanna SK, Rizzino A.** Emerging roles of microRNAs in the control of embryonic stem cells and the generation of induced pluripotent stem cells. *Dev Biol* 344: 16–25, 2010.
29. **Mentzel S, Dijkman HB, Van Son JP, Koenem RA, Assmann KJ.** Organ distribution of aminopeptidase A and dipeptidyl peptidase IV in normal mice. *J Histochem Cytochem* 44: 445–461, 1996.
30. **Metsuyanim S, Harari-Steinberg O, Buzhor E, Omer D, Pode-Shakked N, Ben-Hur H, Halperin R, Schneider D, Dekel B.** Expression of stem cell markers in the human fetal kidney. *PLos One* 4: e6709, 2009.
31. **Micalizzi DS, Farabaugh SM, Ford HL.** Epithelial-mesenchymal transition in cancer: parallels between normal development and tumor progression. *J Mammary Gland Biol Neoplasia* 15: 117–134, 2010.
32. **Nielsen S, Frøkiæ J, Marples D, Kwon TH, Agre P, Knepper MA.** Aquaporins in the kidney: from molecules to medicine. *Physiol Rev* 82: 205–244, 2002.
33. **Oliver JA, Klinakis A, Cheema FH, Friedlander J, Sampogna RV, Martens TP, Liu C, Efstratiadis A, Al-Awqati Q.** Proliferation and migration of label-retaining cells of the kidney papilla. *J Am Soc Nephrol* 20: 2315–2327, 2009.
34. **Oliver JA, Maarouf O, Cheema FH, Martens TP, Al-Awqati Q.** The renal papilla is a niche for adult kidney stem cells. *J Clin Invest* 114: 795–804, 2004.
35. **Panchision DM.** The role of oxygen in regulating neural stem cells in development and disease. *J Cell Physiol* 220: 562–568, 2009.
36. **Pistollato F, Chen HL, Schwartz PH, Basso G, Panchision DM.** Oxygen tension controls the expansion of human CNS precursors and the generation of astrocytes and oligodendrocytes. *Mol Cell Neurosci* 35: 424–435, 2007.
37. **Pleniceanu O, Harari-Steinberg O, Dekel B.** Concise review: kidney stem/progenitor cells: differentiate, sort out, or reprogram? *Stem Cells* 28: 1649–1660, 2010.
38. **Ronco P, Brunisholz M, Geniteau-Legendre M, Chatelet F, Verroust P, Richet G.** Physiopathologic aspects of Tamm-Horsfall protein: a phylogenetically conserved marker of the thick ascending limb of Henle's loop. *Adv Nephrol Necker Hosp* 16: 231–249, 1987.
39. **Sagrinati C, Netti GS, Mazzinghi B, Lazzeri E, Liotta F, Frosali F, Ronconi E, Meini C, Gacci M, Squecco R, Carini M, Gesualdo L, Francini F, Maggi E, Annunziato F, Lasagni L, Serio M, Romagnani S, Romagnani P.** Isolation and characterization of multipotent progenitor cells from the Bowman's capsule of adult human kidneys. *J Am Soc Nephrol* 17: 2443–2456, 2006.
40. **Sallustio F, De Benedictis L, Castellano G, Zaza G, Loverre A, Costantino V, Grandaliano G, Schena FP.** TLR2 plays a role in the activation of human resident renal stem/progenitor cells. *FASEB J* 24: 514–525, 2010.
41. **Simon MC, Keith B.** The role of oxygen availability in embryonic development and stem cell function. *Nat Rev Mol Cell Biol* 9: 285–296, 2008.
42. **Soeda A, Park M, Lee D, Mintz A, Androutsellis-Theotokis A, McKay RD, Engh J, Iwama T, Kunisada T, Kassam AB, Pollack IF, Park DM.** Hypoxia promotes expansion of the CD133-positive glioma stem cells through activation of HIF-1alpha. *Oncogene* 28: 3949–3959, 2009.
43. **Uchida S.** In vivo role of CLC chloride channels in the kidney. *Am J Physiol Renal Physiol* 279: F802–F808, 2000.
44. **Voog J, Jones DL.** Stem cells and the niche: a dynamic duo. *Cell Stem Cell* 6: 103–115, 2010.
45. **Wang X, Dai J.** Concise review: isoforms of OCT4 contribute to the confusing diversity in stem cell biology. *Stem Cells* 28: 885–893, 2010.
46. **Wang Y, Liu Y, Malek SN, Zheng P, Liu Y.** Targeting HIF1α eliminates cancer stem cells in hematological malignancies. *Cell Stem Cell* 8: 399–411, 2011.
47. **Xu N, Papagiannakopoulos T, Pan G, Thomson JA, Kosik KS.** MicroRNA-145 regulates OCT4, SOX2, and KLF4 and represses pluripotency in human embryonic stem cells. *Cell* 137: 647–658, 2009.